Analysis of forced-convection boiling flow instabilities in a single-channel upflow system

T. Doğan*, S. Kakaç† and T. N. Veziroğlu†

A numerical model is developed to predict the steady-state and transient behaviour of forced-convection boiling two-phase flow in a single channel. The model is based on the assumption of homogeneous two-phase flow and thermodynamic equilibrium of the phases. Compressibility effects in the two-phase region, motion of the bulk boiling interface and the thermal capacity of the heater wall have been included in the analysis. The model is used to study the effects of heat input, inlet subcooling and flow rate on the system behaviour. For comparison purposes, an experimental investigation was conducted using a single-channel, electrically heated, forced-convection upflow system. Steady-state operating characteristics, and stable and unstable regions, are determined as a function of heat flux, inlet subcooling and mass flow rate. Different modes of oscillation and their characteristics have been investigated. The model's predictions are in good agreement with the experimental results.

Key words: *convection, two-phase flow, boiling*

In recent years, considerable interest has been expressed in the phenomenon of flow instability in two-phase flow systems. Oscillations of the flow rate and system pressure are undesirable as they can cause mechanical vibrations, high pressures, problems of system control and, in extreme circumstances, disturb the heat transfer characteristics so that the heat transfer surface may burn out. It is essential, therefore, that such instabilities be avoided or controlled in equipment or devices involving two-phase flows. Two-phase flow systems, where these oscillations are critical, occur in a wide range of industrial applications ranging from nuclear reactors to conventional power plants, refrigeration equipment and several chemical process devices. Therefore the understanding of two-phase flow instability is important for the design, control and performance prediction of any system having such phenomena. It is necessary to establish the influence of system geometry, pressure, flow rate, temperature, quality, inlet and exit restrictions, and mass flow rate on the system behaviour, as well as the effects of property variations, the variation of heat flux and the variation of the friction coefficient during the two-phase flow oscillations.

There are three identifiable types of oscillation, namely, the pressure-drop type, the density-wave type, and thermal oscillations which may be encountered in a boiling flow. Each one is associated with a specific mode of operation depending on system characteristics and operational parameters. Detailed discussion of the types and mechanisms of these instabilities is given elsewhere[1–9]. In the present study, the two most observed instabilities, namely, pressure-drop and density-wave oscillations; are discussed. It is important to be able to predict the conditions under which a two-phase flow system will be subject to these instabilities. An analysis of these oscillations involves finding a solution of the governing differential equations subject to initial and boundary conditions. Owing to the complicated nonlinear nature of these equations, numerical methods are invariably used[10–13].

In the analysis of two-phase flows one must employ modelling, the validity of which has to be demonstrated by the comparison of theoretical with experimental results. In the present study a mathematical model is used to simulate the instabilities, and the analysis assumes an equilibrium homogeneous flow. Although the homogeneous model has been used to solve a variety of two-phase flow problems, the main purposes of this work are the prediction of two-phase flow oscillations and a study of the effects of heat input, inlet subcooling and the flow rate on system stability. Pressure-drop and density-wave dynamic instabilities in a two-phase flow system have been simulated. The amplitudes and periods of sustained oscillations and the stability–instability boundaries for a single-channel upflow system at different heat inputs and subcoolings have been predicted, and experiments carried out to justify the model used.

Experimental details

Test apparatus

Fig 1 is a schematic diagram of the boiling upflow system apparatus used in the experiments. It con-

* IMPELL Corp., SED San Francisco, California, USA.
† University of Miami, Coral Gables, Florida 33124, USA.
Received 25 January 1982 and accepted for publication on 15 February 1983.

 0142–727X/83/030145–12$03.00

sisted of a test liquid container, a control valve, a surge tank, an inlet valve, an inlet plenum, a test section, an exit plenum, and an exit restriction. All the tubing in the system, including the heater, was made of nichrome. The test section tube itself was used as the electrical resistance for providing heat input.

The heater was insulated from the rest of the system through ptfe unions at both ends. A direct voltage was applied over two brass flanges, each brazed to one end of the heater, making the electrical resistance of the terminals negligible compared with that of the heater tube. To reduce the heat losses to a minimum, a vacuum chamber was used to house the test section, and a guard heater (incorporating a radiation guard) was built around the heater. This construction kept the heat losses to a level of less than 3 per cent. Three sight glass tubes were included in the system for visual inspection of the flow.

The surge tank was connected to a pressurized air system to maintain a predetermined liquid level in the surge tank. The liquid inlet temperatures could be controlled by a subcooling unit, equipped with automatic temperature controls. During the experiments the liquid in the container was pressurized by high-pressure nitrogen, using a constant pressure regulating valve to maintain the required flow rate into the test section. There was also a recovery system located on the downstream side.

The piping was constructed from 3.75 mm inner diameter nichrome tube, except in the recovery

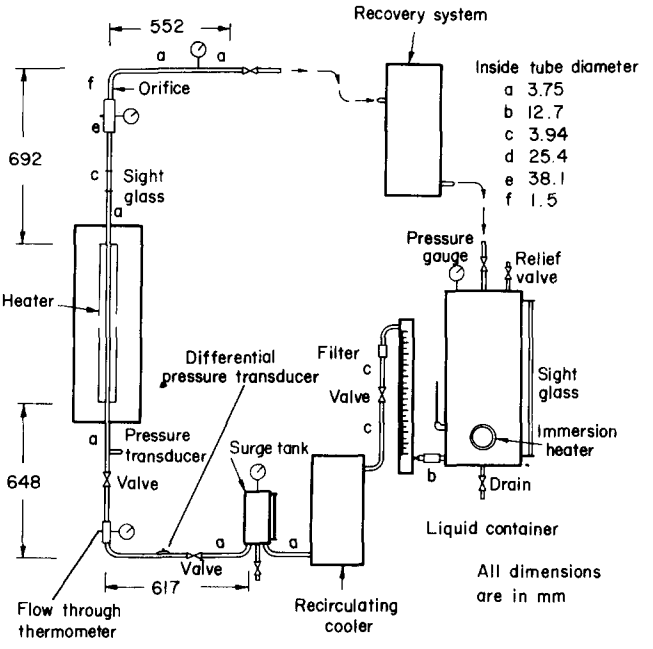

Fig 1 Upward boiling flow apparatus

system. In the recovery section tubing of 25.4 mm inner diameter was used to minimize pressure losses, thus maintaining a near constant level of exit pressure from the test section. Three sight glasses incorporated into the loop helped the visual observation of liquid levels and flow conditions in some critical sections. In particular, the exit sight glass fitted right

Notation

A	Cross-sectional area (m^2)
a	Speed of sound, m/s
b	Boiling length (m)
C	Perimeter (m)
c	Specific heat capacity (kJ/kgK)
c_p	Specific heat capacity at constant pressure (kJ/kgK)
d	Diameter (m)
e	Internal energy (J/kg)
f	Friction factor (dimensionless)
G	Mass flux (kg/m^2s)
g	Gravitational acceleration (m/s^2)
h	Enthalpy (kJ/kg)
Δh_v	Latent heat of vaporization (kJ/kg)
l	Length (m)
m	Mass flow rate (kg/s)
p	Pressure (kN/m^2)
Q	Rate of heat transfer (kJ/s)
q	Rate of heat transfer per unit length (W/m)
$\dot{q}$	Rate of heat generation per unit volume (W/m^3)
R	Frictional resistance coefficient (dimensionless)
S	Suppression factor (dimensionless)
T	Temperature (K)
t	Time (s)
u	Velocity (m/s)
V	Volume (m^3)
$\dot{V}$	Volume flow rate (m^3/s)
x	Flow mixture quality (dimensionless)
z	Axial distance (m)
α	Heat transfer coefficient (W/m^2K)
μ	Dynamic viscosity (kg/ms)
λ	Thermal conductivity (W/mk)
ν	Kinematic viscosity (m^2/s)
ρ	Density (kg/m^3)
ρ_l	Density of liquid (kg/m^3)
ρ_v	Density of vapour (kg/m^3)
σ	Surface tension (N/m)
τ	Shear stress (N/m^2)
ψ	Void fraction (dimensionless)
Nu	Nusselt number, $\alpha d/\lambda$ (dimensionless)
Pr	Prandtl number, $c_p\mu/\lambda$ (dimensionless)
Re	Reynolds number, ud/ν (dimensionless)

Subscripts

a	Air
b	Boiling
c	Convective
e	Exit
h	Heater
l	Saturated liquid
v	Saturated vapour, gas
i	Inlet
i	Spatial index
j	Temporal index
p	Phase
T	Tank
w	Wall

after the heater provided a very clear view of the two-phase flow oscillations.

Flow rate and heat input, and pressure and temperature at appropriate localities, were measured during each run. Temperature measurements were made with standard copper–constantan thermocouples. Five of these, fixed to the outer surface of the heater at 127 mm intervals, were used for heater wall temperature measurements. To avoid floating voltage effects, the thermocouple ends were electrically insulated from the wall surface by 0.4 mm thick mica flakes. Two flow-through thermocouples at the exit side and a third one at the inlet side of the heater were used for fluid temperature measurements at these points.

Pressures were measured at five different points with Bourdon type Heise pressure gauges. In addition, a strain-gauge type pressure transducer was used to record pressure variations at the heater inlet. A calibrated rotameter was used for flow rate measurements. However, the slow response rate of the rotameter made it unsuitable for the measurement of rapid flow variations. Owing to the cushioning effect of the surge tank, oscillations were either much slower or not transmitted at all to the rotameter side. Therefore, the rotameter reading was taken to indicate the average flow rate into the test section. To detect and measure the rapid flow rate oscillations, a differential pressure transducer was used. Taking its signal from a 100 mm straight portion of the inlet pipe, this gauge sensed the frictional pressure drop between the pick-up points, thereby indicating the flow rate.

The outputs of the pressure transducers were fed directly to a four-channel amplifier–recorder unit. The signals, after being amplified in individual amplifiers, drove galvanometer-type styluses. A variable-speed drive for the recorder paper movement, and a time marker, combined with separate gain controls for each channel, permitted detailed recordings of signal histories. Thermocouple outputs were fed selectively, either to a digital voltmeter or to the remaining two channels of the recorder. To eliminate mutual effects, three separate cold junctions were used in the thermocouple circuit.

The heat input was determined by measuring the current and the voltage drop across the heated section.

Experimental procedure

A series of experiments was conducted using Freon-11 as the test fluid. The tests covered a range of inlet subcooling from −9°C to 60°C, heat inputs from 300 W to 700 W and flow rates up to 0.015 kg/s. During the tests the pressure in the heated section ranged from 210 kN/m^2 to 520 kN/m^2, depending on the particular flow conditions. The main tank pressure was kept constant at a suitable pressure between 580 kN/m^2 and 690 kN/m^2, depending on the particular run, and the exit pressure was essentially constant around 110 kN/m^2. System geometry was not altered and good repeatability was obtained for most of the test range.

For each test, the heat input and inlet temperature were chosen as test parameters and the flow rate was varied in small steps to cover the available range. Steady-state characteristics and stability boundaries were determined during each test. Oscillations were identified by the cyclic variation of test-section pressure and flow rate, as indicated by the pressure gauge pointers and also by the recorder. Brief transients were disregarded and only sustained oscillations were considered in defining the stability boundary.

The test procedure can be best summarized by the following steps: (1) With enough liquid in the main tank and the inlet temperature set, the tank was pressurized by nitrogen gas. (2) The flow rate and heat input were increased gradually to the desired starting point, and the system was allowed to become steady as indicated by system pressure, temperature and flow rate. In the meantime, an average liquid level was established in the surge tank by temporarily closing down the inlet valve and by adjusting the surge tank pressure. (3) Measurements of temperature, pressure, flow rate and heat input were taken and critical observations noted. (4) The mass flow rate was reduced by a small amount using the flow control valve. Following each adjustment the system was allowed to become steady, after which step (3) was repeated until sustained oscillations were observed. This procedure was then repeated for different heat inputs and inlet temperatures to cover the allowable range.

The stability boundaries were approached several times during a test with smaller adjustments in flow rate. This eliminated the possibility of crossing directly into the unstable region, which otherwise would cause misleading information regarding the stability boundary. Also worth mentioning is the point that, without exception, the pressure-drop oscillations were encountered first and then the density-wave oscillations. Therefore, after locating the stability boundary for pressure-drop oscillations, tests were continued towards lower mass flow rates, and boundaries for density-wave oscillations were determined in the same way as explained above.

The recorder kept a continuous history of flow variables during each test, thus providing detailed information about the instabilities for later analysis.

Experimental results

Fig 2 shows the pressure drop against mass flow rate, the pressure drop being the pressure difference between the surge tank and the system exit. For low inlet temperatures and at sufficiently high flow rates, where all liquid flow persisted throughout the system, the relation was roughly parabolic, corresponding to turbulent liquid flow. As the flow rate was decreased and net vapour generation started, the trend was reversed and a decrease in flow rate was accompanied by an increase in pressure drop. The negative slope region widened and became less steep at increasingly higher inlet temperatures.

The unsteady state behaviour of the flow system was analysed first by considering the effect of initial flow rate at some particular inlet temperature

and heat input. Under conditions of net vapour generation in the negative slope region, pressure-drop oscillations were observed. Fig 3(a) shows recordings of the typical pressure-drop oscillations. These oscillations were identified by a cyclic change of flow condition and have periods of the order of one minute. As the peak of the $\Delta P/\dot{m}$ curve approached, the pressure-drop oscillations gradually weakened and finally disappeared. The pressure-drop oscillations were always followed by a stable region where no oscillations were observed. The length of this stable region increased with decreasing inlet subcooling, defined as the difference between the inlet temperature and the saturation temperature.

For conditions close to the saturated vapour state at the heater exit (positive slope region on the

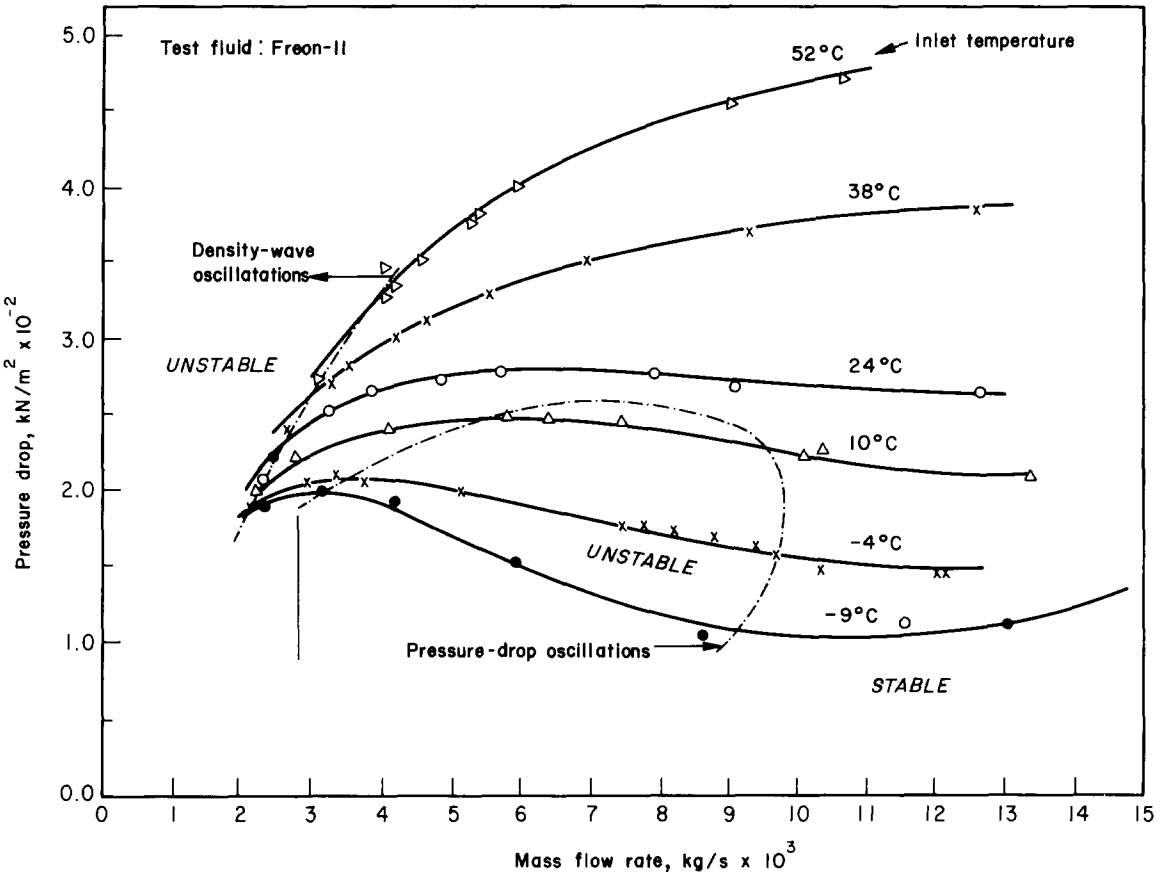

Fig 2 Stability map showing stable and unstable regions for various inlet temperatures at 400 W input

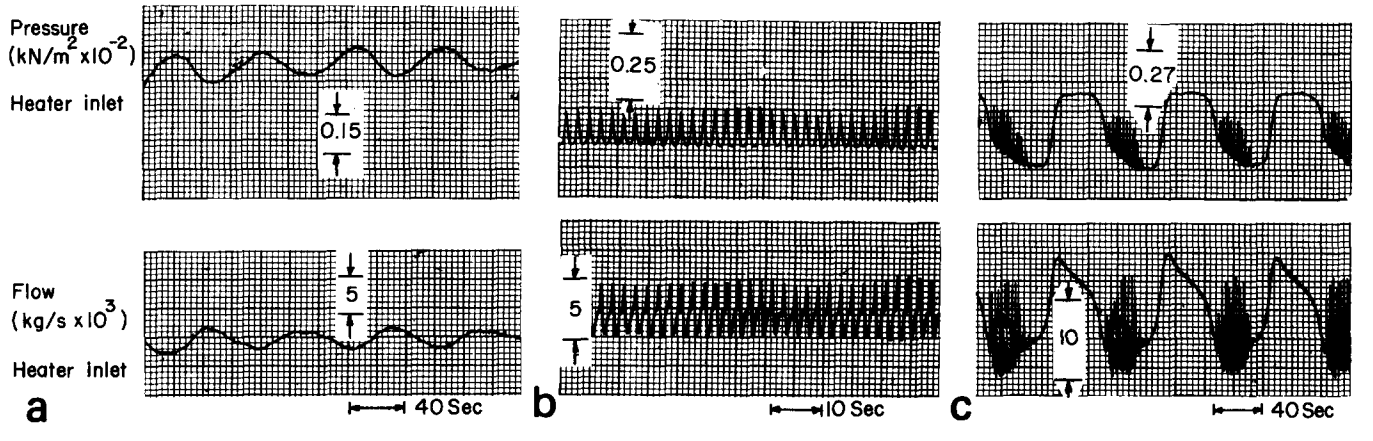

Fig 3 (a) Pressure-drop oscillations (400 W, 9°C inlet, 7.6×10^{-3} kg/s). (b) Density-wave oscillations (400 W, 24°C inlet, 2.42×10^{-3} kg/s). (c) Pressure-drop oscillations with superimposed density-wave oscillations (500 W, −1°C, 6.8×10^{-3} kg/s)

$\Delta P/\dot{m}$ curve), density-wave oscillations are observed. These oscillations were more violent than the pressure-drop oscillations and had periods of the order of one second, as shown in Fig 3(b).

The pressure-drop oscillations were not always in pure form. Under certain flow conditions they appeared in combination with density-wave oscillations, as shown in Fig 3(c). Such oscillations were observed generally with high heat inputs. The density-wave oscillations appeared only in the low flow rate part of the cycle. A detailed presentation of the experimental programme and results is given in Refs 14 and 15.

3. Mathematical formulation

The one-dimensional transient conservation equations which are used to describe the two-phase flow inside the constant area channel used in the experiments are based on a homogeneous equilibrium model. This model assumes the liquid–vapour mixture to be homogeneous and the phases in the mixture to be in thermodynamic equilibrium. The resulting conservation equations are similar to those for single-phase flow, but the constitutive relations are quite different. These relations, i.e. two-phase friction and heat transfer correlations, and the density changes account for the two-phase phenomena.

Conservation equations

The conservation laws for mass, momentum and energy as applied to one-dimensional, unsteady homogeneous viscous flows can be written as[14,16]:

Continuity:

$$\frac{\partial \rho}{\partial t}+\frac{\partial G}{\partial z}=0 \tag{1}$$

Momentum:

$$\frac{\partial G}{\partial t}+\frac{\partial}{\partial z}\left[\frac{G^2}{\rho}\right]=-\frac{\partial p}{\partial z}-\rho g-2\frac{f}{d}\frac{G^2}{\rho} \tag{2}$$

Energy:

$$\frac{\partial}{\partial t}(\rho e)+\frac{\partial}{\partial z}(Gh)=\frac{4}{d}\alpha(T_w-T_l) \tag{3}$$

with

$$\rho=\rho_v/\left[x+(1-x)\frac{\rho_v}{\rho_l}\right] \tag{4}$$

$$h=(1-x)h_l+xh_v \tag{5}$$

The subscripts l and v refer to the liquid and vapour phases, respectively. The equations are written for a uniform flow area of diameter d, and the kinetic and potential energy terms have been neglected. Furthermore, in the energy equation the rate of change of internal energy e is assumed to be equal to the rate of change of enthalpy h.

The above set of equations is closed by adding the constitutive equations which are given in the following sections.

Two-phase friction coefficient

In line with the assumption of homogeneous flow, a section of two-phase region can be imagined to be composed of alternative slices of liquid and vapour. The total wall friction force per unit length can then be expressed as the sum of the frictional forces due to liquid and vapour phases. Thus:

$$\tau_w C=\tau_{wl}C_l+\tau_{wv}C_v \tag{6}$$

where C_l and C_v are the liquid and vapour wetted perimeters given by:

$$C_l=(1-\psi)C \qquad C_v=\psi C \tag{7}$$

where ψ is the void fraction. On substituting Eq (6) into Eq (5) one obtains:

$$\tau_w=(1-\psi)\tau_{wl}+\psi\tau_{wv} \tag{8}$$

When we assume that τ_{wl} and τ_{wv}, the wall shear stresses for the liquid and vapour, are given by Fanning's relation for the corresponding phases, then Eq (8) can be put into a form similar to the single phase relationship:

$$\tau_w=\frac{1}{2}f\rho u^2 \tag{9}$$

where

$$f=(1-\psi)\frac{\rho_l}{\rho}f_l+\psi\frac{\rho_v}{\rho}f_v \tag{10}$$

The friction factors f_l and f_v in Eq (10) are calculated from the well-known correlations of Moody:

$$f_p=0.079\left(\frac{\rho_p u d}{\mu_p}\right)^{-0.25}, \qquad p=l, v \tag{11}$$

In our experimental set-up, the heater was not very long (about 80 cm); it is found that the contribution of this working section to the total system pressure drop (between the surge tank and the exit restriction) is very small. The main pressure drop occurs at the exit restriction, which is an important component of the set-up in the instability analysis. Therefore, the effect of the friction coefficient in the heater is virtually negligible in our case.

Heat transfer coefficient

The heat input into the fluid is given by

$$Q=\alpha A_h(T_w-T_l) \tag{12}$$

where A_h is the heater surface area, T_l is the fluid temperature and T_w is the heater wall temperature. The expression for the heat transfer coefficient α, however, is much more involved. The complication arises mainly from the existence of boiling which may assume different modes depending on the heater surface, the magnitude of the heat flux, the type of fluid and the flow conditions. As a result, the effective heat transfer coefficients can be quite different from the corresponding single-phase heat transfer coefficient. To account for this variation several mechanisms and equations have been suggested. The usual procedure is to define two-phase multipliers and/or correction factors. Yet, the resulting equations have been used with limited success only.

The overall heat transfer coefficient is assumed to be composed of a microconvective term α_b, and a macroconvective term α_c, based on Chen's correlation[17,18]. Thus:

$$\alpha = \alpha_b + \alpha_c \tag{13}$$

By extending the analysis of Forster and Zuber[18,19] for pool boiling, Chen derived an expression for α_b as:

$$\alpha_b = 0.00122\left[\frac{\lambda_f^{0.79} c_{pl}^{0.45} \rho_l^{0.49} g^{0.25}}{\sigma^{0.25} \mu_l^{0.29} \Delta h_v^{0.24} \rho_v}\right] \times (\Delta T)^{0.24} (\Delta p)^{0.75} S \tag{14}$$

In this expression S is called the suppression factor and accounts for superheat variation within the boundary layer; it has a value between zero and unity.

In this study, Eq (14) is assumed to apply for both the saturated and the subcooled boiling regions. The factor S is taken as unity for qualities up to 0.30. Beyond this, for numerical solutions it is approximated by a parabolic curve, becoming 0.4 at $x = 1.0$, which is in accordance with Fig 7.6 of Ref 18. The macroconvective heat transfer coefficient, on the other hand, is assumed to be contributed proportionately from the liquid and vapour regions. Using a similar logic to that for the wall friction coefficient above:

$$\alpha_c = (1-\psi)\alpha_l + \psi\alpha_v \tag{15}$$

where α_l and α_v are calculated from the Dittus–Boelter equation:

$$\alpha_p = 0.023\left(\frac{\rho_p u d}{\mu_p}\right)^{0.8}\left(\frac{c_p \mu_p}{\lambda_p}\right)^{0.4}\frac{\lambda_p}{d}, \qquad p = l, v \tag{16}$$

Since the coefficient α_b is not directly dependent on the flow rate, it can be seen from Eq (13) that the heat transfer coefficient has flow dependent and flow independent components.

The heater wall temperature T_w in Eq (12) is obtained from an energy balance of the heater itself:

$$(\rho c A)_w \frac{dT_w}{dt} = \dot{q} A_w - \alpha C (T_w - T_l) \tag{17}$$

where $\dot{q}$ is the heat generation rate per unit volume of the tube material, A_w is the wall cross-sectional area, C is the inner perimeter of the tube, and ρ and c are the density and specific heat, respectively, of the tube material.

The bulk boiling boundary

When the above set of equations is applied, a distinction must be made between the two-phase and liquid regions. This is done by defining a bulk boiling boundary, ie the point where the bulk liquid temperature reaches the local saturation temperature. For a linear variation of both h and h_l in the vicinity of the boiling boundary b, the enthalpy profiles can be approximated as (see Fig 4):

$$h = (h_0 + \Delta h) + \frac{\partial h}{\partial z}\Delta z \tag{18}$$

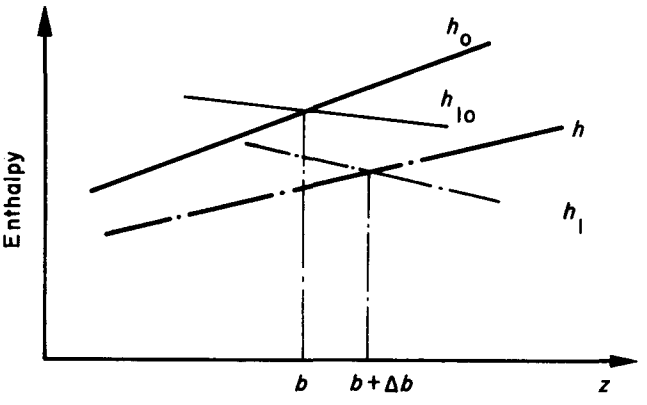

Fig 4 Variation of enthalpy along the channel during the transients

$$h_l = (h_{l0} + \Delta h_l) + \frac{\partial h_l}{\partial z}\Delta z \tag{19}$$

Since at the bulk boiling boundary $h = h_l$, and $h_0 = h_{l0}$, the change in subcooled length Δb is:

$$\Delta b = \left.\frac{\Delta h_l - \Delta h}{\partial h/\partial z - \partial h_l/\partial z}\right|_b \tag{20}$$

where Δb is the displacement of the bulk boiling boundary. If the local variation of pressure is small compared with the absolute value of the pressure, the term Δh_l can be neglected. Hence:

$$\Delta b = -\left.\frac{\Delta h}{\partial h/\partial z - \partial h_l/\partial z}\right|_b \tag{21}$$

with

$$\left.\frac{\partial h}{\partial z}\right|_{b,t} = \left.\frac{\partial h}{\partial z}\right|_{0,t-t_0} \tag{22}$$

$$\left.\frac{\partial h_l}{\partial z}\right|_{b,t} = \left.\frac{\partial h_l}{\partial p}\frac{dp}{dz}\right|_{b,t} \tag{23}$$

where t_0 is the solution of

$$b = \int_{t-t_0}^{t} u(t)\,dt \tag{24}$$

A velocity for the boiling boundary can be defined as:

$$u_b = \frac{\Delta b}{\Delta t} \tag{25}$$

where Δb is given by Eq (21). It must be noted that u_b cannot be greater than the particle velocity since this would require very high condensation rates. Therefore $u_b \leq u_p$, where u_p is the particle velocity at the boiling boundary.

Surge tank dynamics

The flow system of Fig 1 contains two additional elements that must be considered. The first element is the surge tank that provides a compressible volume at the upstream section. The second element is a flow restriction fitted at the system exit to provide an additional pressure drop. These will be discussed below.

For given inlet conditions the temperature of the liquid in the surge tank can safely be assumed constant. This ensures constant partial pressure of the vapour in the compressible volume. For the surge tank, the continuity equation may be written as:

$$\dot{V}_i - \dot{V}_o - \dot{V}_{ev} = \frac{dV_l}{dt} \tag{26}$$

where $\dot{V}_{ev}$ is the rate of loss of liquid volume due to evaporation in the surge tank, $\dot{V}_i$ and $\dot{V}_o$ are the rates of volume flow into and out of the surge tank. Since the sum of the liquid volume V_l and gas volume V_T in the surge tank is constant, we write:

$$\frac{dV_l}{dt} = -\frac{dV_T}{dt} \tag{27}$$

The rate of loss of liquid volume due to evaporation in the surge tank (from continuity) is:

$$\dot{V}_{ev} = \frac{\rho_v}{\rho_l}\frac{dV_T}{dt} \tag{28}$$

On substituting Eqs (27) and (28) into Eq (26) we obtain:

$$\dot{V}_i - \dot{V}_o = \left(\frac{\rho_v}{\rho_l} - 1\right)\frac{dV_T}{dt} \tag{29}$$

Since for temperatures lower than the critical temperature $(\rho_v/\rho_l) \ll 1$, integration of Eq (29) yields:

$$V_T = \int_0^t (\dot{V}_i - \dot{V}_o)\, dt \tag{30}$$

For a perfect gas, we can state:

$$P_a V_T = P_{a0} V_{T0} \tag{31}$$

where the subscript 0 refers to the initial conditions and P_a is the partial pressure of air. Since the gas in the surge tank is a mixture of air and saturated vapour, we have:

$$P_T = P_a + P_v \tag{32}$$

where P_T is the surge tank pressure and P_a and P_v are partial pressures of the air and vapour, respectively.

On eliminating P_a between Eqs (31) and (32) and introducing V_T from Eq (30), we obtain:

$$P_T = P_v + (P_{T0} - P_v)V_{T0} \Big/ \int_0^t (\dot{V}_i - \dot{V}_o)\, dt \tag{33}$$

If P_v is negligible in comparison with P_{T0}, Eq (33) reduces to:

$$P_T = P_{T0} V_{T0} \Big/ \int_0^t (\dot{V}_i - \dot{V}_o)\, dt \tag{34}$$

Pressure loss through exit restriction

The exit restriction which terminates the test section contributes a large portion of the total pressure drop. It is basically an abrupt contraction followed by an abrupt expansion. An empirical relation which gives the pressure drop through this element is obtained as:

$$\Delta P_e = 142\left(1 + x\frac{V_{lv}}{V_l}\right)\frac{G^2 V_l}{2} \tag{35}$$

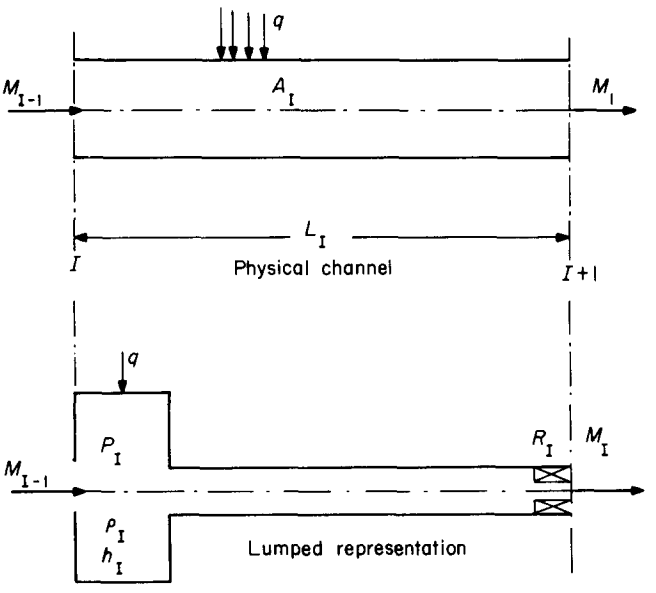

Fig 5 Lumped representation of a channel segment

The fluid properties are assumed to be known functions of either pressure or enthalpy or both. These functions have been developed in the form of polynomials using the fluid tables.

The above equations together with the equation of state are solved for a constant exit pressure, which was ensured by the low frictional resistance of the exit ducting and by a vent from the recovery tank to the atmosphere. In addition, constant flow rate into the surge tank and constant heat generation in the heater were confirmed during the experiments.

Method of solution

Eq (1)–(35) complete the set of equations necessary to describe the flow system of Fig 1. These equations are solved using a lumped-parameter approach. The basic idea of the method is to view the flow system as a finite number of segments. The flow variables then are assumed to be represented by appropriate average values over each segment. Fig 5 shows a section of the actual flow channel and its equivalent lumped representation. This representation is sometimes called 'fluid transmission line', because it is analogous to a transmission line with capacitance, inductance and resistance. Energy and mass conservation equations are applied for the tank, and a momentum equation for the tube.

The method has been successfully used by several investigators for modelling single-phase and two-phase flows. Redfield and Murphy[20] used the method for simulating reactor accidents. The computer code RELAP-4[21], which was developed for reactor accident analysis, uses the 'tube and tank' model.

In this study, the test section of Fig 1 is represented by five lumps. If boiling occurs then that segment is further divided into two segments to separate the liquid region from the two-phase region. The resulting lumped-parameter representation of

the system is shown in Fig 6. The differential equations are replaced by their algebraic equivalents, and steady- and unsteady-state solutions are obtained. The following sections outline the numerical schemes for both cases.

Steady-state equations

Referring to Fig 6 and noting that each segment has the same cross-sectional area, the steady-state governing equations can be written as follows:

Continuity equation:

$$G = G_{i-1} \tag{36}$$

Momentum equation:

$$P_i = P_{i-1} - \left[\rho_i g + R_i \frac{2f_i}{d}\frac{G_i^2}{\rho_i} + \frac{G_i^2}{l_i}\left(\frac{1}{\rho_i} - \frac{1}{\rho_{i-1}}\right)\right] l_i \tag{37}$$

Energy equation:

$$h_i = h_{i-1} + \frac{q_i l_i}{G_i A} \tag{38}$$

Equation of state:

$$\eta_i = f(h_i) \tag{39}$$

where η_i represents some fluid property.

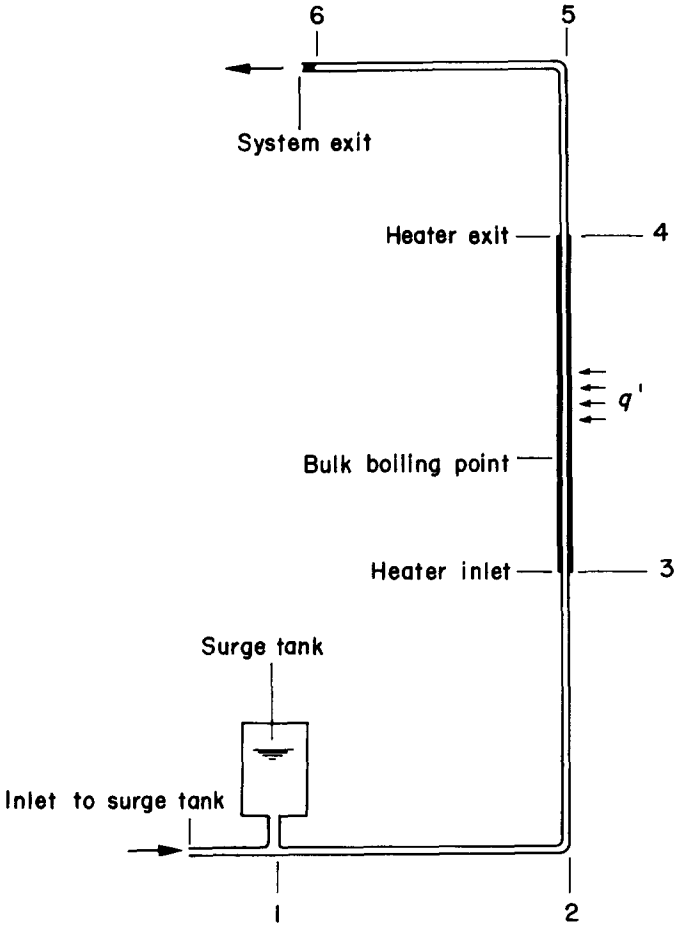

Fig 6 Lumped-parameter equivalence of the actual flow system

The heater wall temperature can be written, from Eq (17), as:

$$T_{wi} = T_i + \frac{q_i l_i}{A\alpha_i} \tag{40}$$

where A is the cross-sectional area of the tube, and q_i is the heat input per unit length of the tube.

The friction coefficient f_i and the heat transfer coefficient α_i are obtained from Eqs (10) and (13) for each segment for the particular conditions of that segment. At each step the liquid enthalpy is checked against the saturation enthalpy and appropriate equations are chosen according to whether the fluid is subcooled, two-phase or superheated.

Calculations start with given values of G_1, T_1, q and p_e. An estimated value for P_1 is taken and the enthalpy, pressure and density at each successive node are calculated. After calculating the exit pressure it is checked against the given value, p_e. If the difference is found to be within an acceptable limit, the calculated value is substituted for p_e; otherwise a new corrected value is taken for P_1 and the whole procedure is repeated. The steady-state solution provides pressure, enthalpy and density at each segment, and also the location of the bulk-boiling boundary.

Unsteady-state equations

An explicit forward difference scheme is used for the unsteady solution. Initial and boundary conditions are obtained from the steady-state solution. The resulting equations, referring to Fig 6, can be written from the lumped-parameter equations given in the earlier mathematical formulation as follows:

Continuity equation:

$$p_i^{j+1} = \rho_i^j - \Delta t(G_i^j - G_{i-1}^j)/l_i \tag{41}$$

Momentum equation (liquid region): Since in the liquid region $\partial G/\partial z = 0$, a single integral momentum equation for the whole liquid region is solved to find the flow rate:

$$G_i^{j+1} = G_i^j + \Delta t\left[(p_1^j - p_b^i) - \sum_1^{b-1} \rho_i^j g l_i - \sum_1^{b-1} R_i 2f_i^j \frac{\rho_i}{d}(G_1^j)^2\right] \Big/ \sum_1^{b-1} l_i \tag{42}$$

with

$$G_1^j = G_2^j = \cdots = G_{b-1}^j$$

Then the individual pressures are found from the segment momentum equations as:

$$p_i^{j+1} = p_{i-1}^{j+1} - \left[\rho_i^j g + R_i \frac{2f_i^j}{d}(G_i^j)^2 + \frac{\partial G_1^j}{\partial t}\right] l_i \tag{43}$$

where

$$\frac{\partial G}{\partial t} = (G_1^{j+1} - G_1^j)/\Delta t \tag{44}$$

Momentum equation (two-phase and superheated region):

$$G_i^{j+1} = G_i^j - \Delta t\left[(p_i^j - p_{i-1}^j) + \rho_i^j g l_i + 2f_i^j \frac{l_i}{d}(G_i^j)^2/\rho_i^j + (G_i^j)^2\left(\frac{1}{\rho_i^j} - \frac{1}{\rho_{i-1}^j}\right)\right]\Big/ l_i \tag{45}$$

In using this equation, an exception is made for the exit segment (segment 5). Here the accelerational pressure drop is negligible compared with the large frictional pressure drop of the exit restriction. Therefore, quasi-steady conditions are assumed to apply for segment 5. The mass flow rate is then calculated from Eq (35) as:

$$G_5^j = \left[(p_5^{j-1} - p_e)\Big/\left\{\left(1 + x\frac{V_{ev}}{V_l}\right)_5^{j-1} \cdot 71.0 \cdot V_l\right\}\right]^{0.5} \tag{46}$$

Energy equation:

$$(\rho h)_i^{j+1} = (\rho h)_i^j - \Delta t\left\{\left[(Gh)_i^j - (Gh)_{i-1}^j\right]\Big/ l_i + q_i^j l_i/A\right\} \tag{47}$$

with

$$\dot{q}_i^j = (\alpha)_i^j \pi d(T_{wi}^j - T_i^j) \tag{48}$$

where α is the heat transfer coefficient.

The enthalpy is then obtained as:

$$h_i^{j+1} = (\rho h)_i^{j+1}/\rho_i^{j+1} \tag{49}$$

The heater wall temperature is obtained from Eq (17) as:

$$(T_w)_i^{j+1} = (T_w)_i^j + \Delta t\left(\dot{q} - \frac{q_i^j}{A_w}\right)\Big/(\rho c)_w \tag{50}$$

Equation of state:

$$p_i^j = f(h_i^j) \tag{51}$$

The surge tank pressure, from Eq (34), is:

$$p_1^{j+1} = p_1^0 V_1^0/V_1^{j+1} \tag{52}$$

where V_1^{j+1} can be calculated from Eq (30) as:

$$V_1^{j+1} = V_1^j + \Delta t A(G_1^j - G_1^0)/\rho_1^j \tag{53}$$

The displacement of the bulk-boiling boundary is now substituted from Eq (21):

$$b^{j+1} = b^j - (h_{b-1}^{j+1} - h_{b-1}^j)/\left(\frac{\partial h}{\partial z} - \frac{\partial h_l}{\partial z}\right)_b^{j+1} \tag{54}$$

with

$$\left(\frac{\partial h_l}{\partial z}\right)_b^{j+1} = \left(\frac{\partial h_l}{\partial p}\right)_b^{j+1}\left(\frac{p_{b-1}^{j+1} - p_b^{j+1}}{l_{b-1}}\right) \tag{55}$$

and

$$\left(\frac{\partial h}{\partial z}\right)_b^j = \left(\frac{q}{GA}\right)_{b-1}^{j-n} \tag{56}$$

where n is given by the solution of

$$b^j = \sum_{k=j}^{j-n}\left(\frac{G_1^k}{\rho_1^k}\right)\Delta t, \qquad n \geq 0 \tag{57}$$

The velocity of the boiling boundary is then:

$$u_b^{j+1} = \frac{b^{j+1} - b^j}{\Delta t}, \qquad u_b^j \leq u_p^j \tag{58}$$

When u_b^j exceeds the particle velocity u_p^j, the boiling boundary location is corrected as:

$$b^{j+1} = b^j + \Delta t \cdot u_b^{j+1} \tag{59}$$

Segment b, the two-phase region next to the boiling boundary, requires special considerations because of the volume change caused by boundary movement. Using the Reynolds transport theorem[22], proper forms of the continuity and energy equations for segment b are:

$$\rho_b^{j+1} = \rho_b^j + \Delta t(G_{in} - G_e)/b \tag{60}$$

and

$$(\rho h)_b^{j+1} = (\rho h)_b^j + \Delta t\left[(G_{in}h_{i-1}^j - G_e h_i^j)/b + \frac{q_i^j}{A}\right] \tag{61}$$

where

$$G_{in} = G_{b-1}^j - u_b^j \rho_{b-1}^j \tag{62}$$

and

$$G_e = G_b^j - u_b^j \rho_b^j \tag{63}$$

In all of the above equations, the time steps were selected so as to conform with the following condition:

$$\Delta t = \frac{\Delta l}{a + |u|} \tag{64}$$

The speed of sound a has an average value of 152 m/s for the saturated vapour at the conditions of interest. At low qualities, it decreases to a value of around 30 m/s. Rather than using variable time steps a constant value of $t = 0.002$ s has been used for high-quality flow conditions (density-wave oscillations). The relatively lower speed of sound for low-quality mixtures allowed for higher time increments. Consequently $t = 0.005$ s was used for those flow conditions.

In summary, the algorithm used in obtaining the unsteady response of the system can be summarized as follows:

Step 1. Obtain the steady-state solution by solving steady-state equations.
Step 2. Give a perturbation to the inlet flow rate.
Step 3. Estimate the inlet conditions from the surge tank equations.
Step 4. Estimate the boiling location, using Eqs (54)–(59).
Step 5. Obtain the transient response of the system by solving the unsteady, lumped-parameter equations. The criterion for the time step is given by Eq (64).

Results and discussion

The dependence of the steady-state pressure on the mass flow was predicted reasonably well by the

model (see Fig 7). Both the experimental and theoretical plots indicate a region of negative slope, characteristic of a boiling flow system. The constant-temperature curves merge asymptotically to a single curve as all-vapour or liquid flow conditions are reached.

Pressure-drop type oscillations

The conditions provided by the steady-state solution are used as the initial conditions for the time-dependent solution. The boundary conditions are constant exit pressure and constant inlet flow rate to the surge tank. A solution is sought by disturbing the system by slightly perturbing the surge tank pressure. The results of the unsteady solutions are in reasonable agreement with the experimental ones. The system is fully stable on the positive-slope region of the pressure-drop curve where there is no boiling. After a very short transient, the system sets itself at steady conditions, and no further oscillations are observed. However, as the flow rate is reduced below a certain value, net vapour generation starts and the slope of the pressure drop curve changes sign. This region of negative slope is unstable and oscillations are observed in the flow variables. Fig 8 is a plot of such oscillations. The experimental recording corresponding to this case is also given for comparison purposes. As can be seen, the predicted amplitudes are lower than the observed amplitudes. The periods, however, are in good agreement with experimental results. The tendency of increasing periods at comparatively lower flow rates is observed both experimentally and analytically.

Density-wave type oscillations

At higher qualities, as the saturated vapour conditions are approached, the slope of the pressure-drop curve changes sign, becoming positive again. This region is also stable and is predicted so by the model. However, as the flow rate is further decreased, new

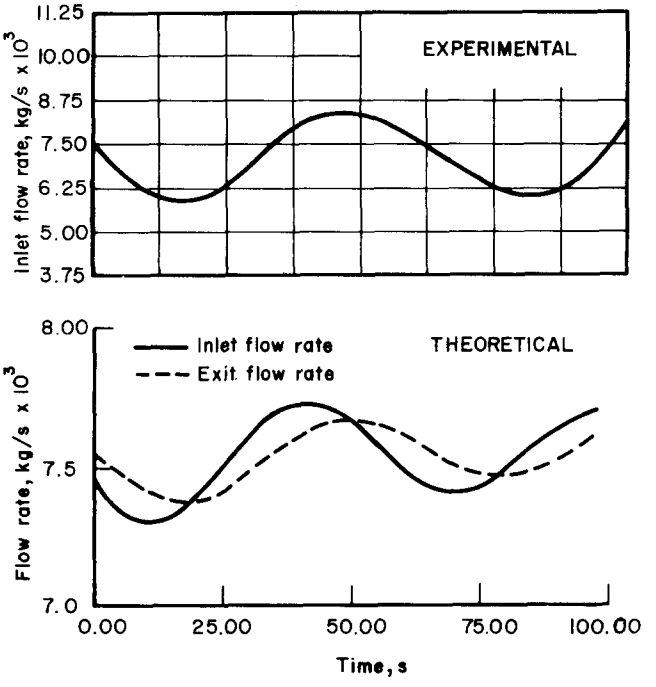

Fig 8 Experimental and predicted pressure-drop oscillations (400 W, 10°C, 7.6×10^{-3} kg/s)

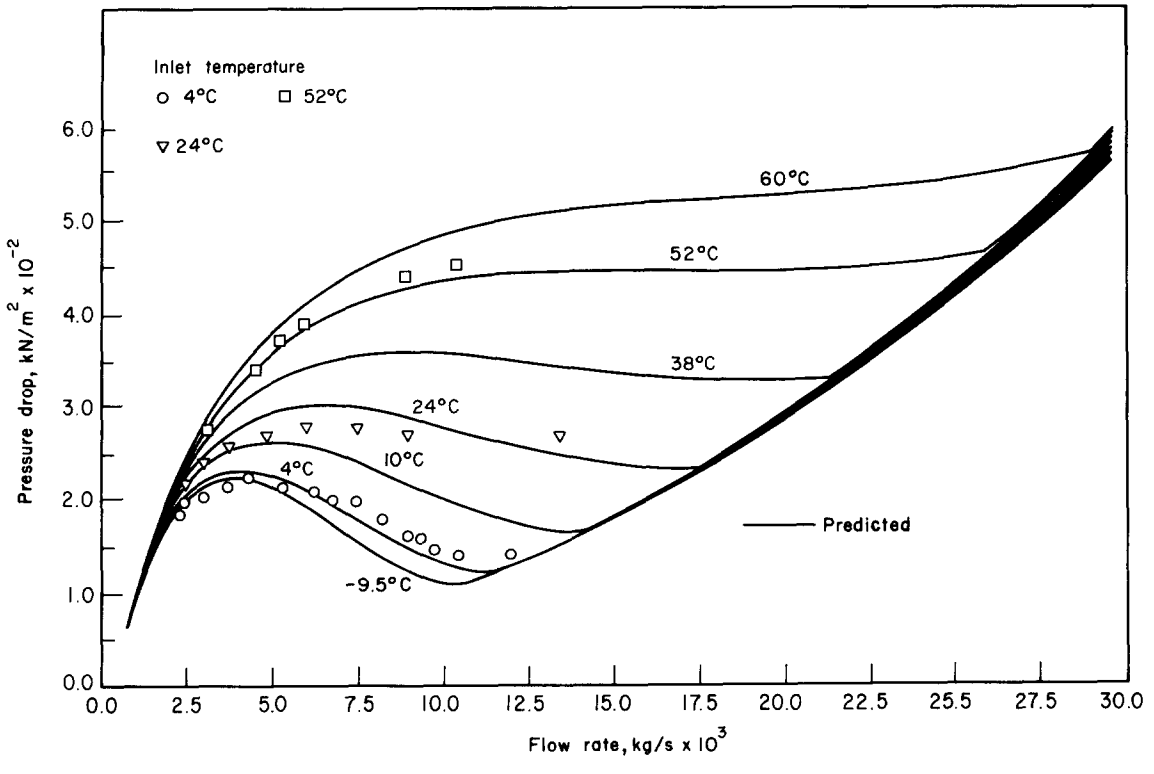

Fig 7 Predicted steady-state pressure-drop characteristics at various inlet temperatures and for 400 W input

oscillations are observed. The character of these oscillations is completely different from the previous one. They have much higher frequencies (of the order of 1 Hz), are more violent, and resemble the density-wave oscillations of the experiments. Fig 9 is a plot of such oscillations with experimental recordings taken under the same conditions. The predicted frequencies are the same as the experimentally observed frequencies. However, the predicted amplitudes of the oscillations are lower than the experimentally observed amplitudes.

More detailed information can be found in Ref 23.

Conclusions

The homogeneous phase equilibrium model can predict the instability boundaries for density-wave and pressure-drop oscillations in forced-convection upflow systems. The same model is also satisfactory for simulating the experimentally observed characteristics of the oscillations and, therefore, can be used in predicting the character of the oscillations for different heat inputs, mass flow rates and inlet temperatures within acceptable accuracy. Different kinds of fluids with properly defined property functions can also be studied.

The results of the foregoing theoretical analysis verify the following facts.

(1) The variation of heat input into the fluid plays an important role in generating and sustaining the pressure-drop oscillations.

(2) The compressible air–vapour mixture located at the upstream side of the system is equally important in sustaining the pressure-drop oscillations.

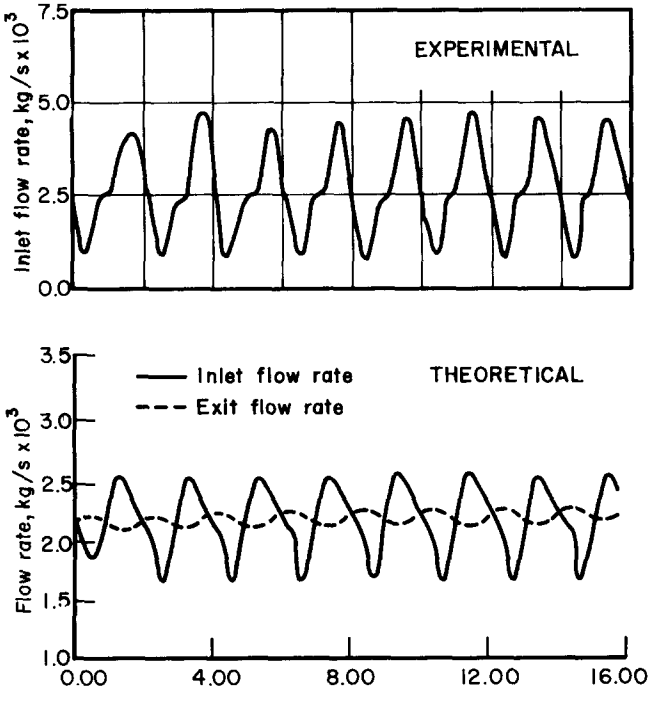

Fig 9 Experimental and predicted density-wave type oscillations (400 W, 24°C, 2.12 × 10⁻³ kg/s)

(3) The negative-slope region widens and becomes less steep at higher inlet temperatures.

(4) Heat input has a direct influence on the character of the oscillations. The variation in heat transfer into the fluid is relatively small for density-wave oscillations.

(5) The compressibility of the two-phase mixture must be included in the mathematical formulations of density-wave oscillations.

(6) The agreement between the experimental results and the predictions of the theory is satisfactory. It is observed that the theory generally underpredicts the pressure drop. The maximum deviation, however, is less than 10 per cent and is observed in the low and intermediate quality ranges.

(7) Stable and unstable regions for both types of oscillation are predicted within reasonable limits for most of the flow conditions. For pressure-drop oscillations and density-wave oscillations, the predicted frequencies are the same as the experimentally observed frequencies; however, the predicted amplitudes of the oscillations are lower than the experimentally observed amplitudes.

In this analysis, the slip between the phases has been neglected. It was found experimentally that when the density-wave oscillations started the value of the quality x was greater than or equal to 0.90. Therefore, for prediction of the density-wave oscillations, the homogeneous flow assumption is a simple and reliable one.

A number of studies have also been conducted on a linearized perturbation analysis of a constant-property homogeneous model[24,25]. The study of instability thresholds in a single boiling channel has also been studied with a variable drift-flux model[25].

Comparison of the experimental and theoretical results shows that the drift-flux formulation offers a simple and reliable way of determining the instability thresholds. The homogeneous flow model provides a good physical understanding of the problem.

Acknowledgements

The authors gratefully acknowledge the financial support of the National Science Foundation of the USA and the Scientific Affairs Division of NATO. The authors wish to thank Messrs Aykut Menteş, H. Gürgenci, O. T. Yıldırım, L. Q. Fu and Z. Lin for their suggestions and assistance in the preparation of the manuscript.

References

1. **Stenning A. H.** Instabilities in the flow of a boiling liquid. *J. Basic Eng., Trans. ASME, 1969, Series D,* 86, *213–217*
2. **Stenning A. H. and Veziroglu T. N.** Flow oscillation modes in forced-convection boiling. *Proc. Heat Transfer and Fluid Mech. Institute, 1965,* pp. 301–306.
3. **Stenning A. H., Veziroglu T. N. and Callahan G. M.** Pressure-drop oscillations in forced convection flow with boiling. *EURATOM Sym. on Dynamics of Two-Phase Flows, 1967*
4. **Veziroglu T. N. and Lee S. S.** Instabilities in boiling upward flows. *Int. Symp. on Research on Concurrent Gas-Liquid Flow, 1968*

5. **Kakaç S., Veziroglu T. N., Aksu H. B. and Alp Y.** Boiling flow instabilities in boiling upward flows. *Int. Symp. on Research on Concurrent Gas-Liquid Flow, FRG, 1968*
6. **Bouré J. A., Bergles A. E. and Tong L. S.** Review of two-phase flow instability. *Nucl. Eng. Design, 1973,* **25**, *165–192*
7. **Kakaç S., Veziroglu T. N., Akyüzlü K. and Berkol O.** Sustained and transient boiling flow instabilities in a cross-connected four-parallel channel upflow system. *Fifth Int. Heat Transfer Conf., Tokyo, Japan, 1974, Paper B5.11*
8. **Bergles A. E.** Review of instabilities in two-phase systems. *Proc. NATO Advanced Study Institute, 1977,* **1**, *382–422. Hemisphere Publishing Corp., Washington DC*
9. **Veziroglu T. N. and Kakaç S. (eds.)** Two-phase transport and reactor safety. *Proc. Two-Phase Flow and Heat Transfer Symp. 1977,* **2**. *Hemisphere Publishing Corp., Washington DC*
10. **Meyer J. R. and Rose R. P.** Application of a momentum integral model to the study of parallel channel boiling flow oscillations. *J. Heat Transfer, Trans. ASME Series C, 1963,* **85**, *1–9*
11. **Lyckowski R. W.** Numerical techniques for the computation of transient unequal phase velocity, unequal phase temperature, two-phase flow and heat transfer, two-phase transport and reactor safety. *Proc. Two-Phase Flow and Transfer Symp., 1977,* **2**, *839–888. Hemisphere Publishing Corp., Washington DC*
12. **Lycowski R. W., Gidaspow A., Solbrig C. W. and Hughes E. D.** Characteristics and stability analysis of transient one-demensional two-phase flow equations and their finite difference approximations. *ASME Paper 75-WA/HT-23*
13. **Akyüzlü K., Veziroglu T. N., Kakaç S. and Dogan T.** Finite difference analysis of two-phase flow pressure-drop and density-wave oscillations. *Wärme- und Stoffubertragung, 1980,* **14**, *253–267*
14. **Doğan T.** Lumped-parameter analysis of two-phase flow instabilities. *PhD Thesis, University of Miami, Miami, Florida, USA, 1979*
15. **Akyüzlü K. M.** Mathematical modelling of two-phase flow oscillations. *PhD Thesis, University of Miami, Miami, Florida, USA, 1979*
16. **Yadigaroglu G. and Lahey R. T.** On the various forms of the conservation equations in two-phase flow. *Int. J. Multiphase Flow, 1976,* **2**, *477–494*
17. **Chen J. C.** A correlation for boiling heat transfer to saturated fluids in convective flow. *ASME Paper 63-HT-34*
18. **Collier J. G.** Convective boiling and condensation. *McGraw-Hill, New York, 1972*
19. **Forster H. K. and Zuber N.** Dynamics of vapor bubbles and boiling heat transfer. *AICE J. 1955,* **1**, *531–535*
20. **Redfield J. A. and Murphy J. H.** Sectionalized compressible and momentum integral models for channel hydrodynamics. *ASME Paper 71-HT-14*
21. **Moore K. V. and Retting W. H.** RELAP 4-A computer program for transient thermal-hydraulic analysis. *Aerojet Nuclear Company, National Reactor Testing Station, A NCR-1127, 1973*
22. **Potter C. M. and Foss J. F.** Fluid mechanics. *Ronald Press Co., New York, 1975*
23. **Veziroglu T. N. and Kakaç S.** Two-phase flow instabilities: the effect of inlet subcooling. *Final Report, NSF Project Eng., 1979, 75-16618*
24. **Davies A. L. and Potter R.** Hydraulic stability, an analysis of the courses of unstable flow parallel channels. *Proc. Symp. Two-Phase Flow Dynamics, Eindhoven, Netherlands, 1977*
25. **Gürgenci H., Veziroglu T. N. and Kakaç S.** Pressure-drop and density-wave instability thresholds in boiling channels. *Sixteenth South Eastern Seminar on Thermal Sciences. Hemisphere Publishing Corp., New York, 1983*